Enhanced Ballistic Trajectory Estimation from Radar Data Using the Cubature Kalman Filter

Daniel Miñan de Oliveira Crus, João Abdalla Ney da Silva, and José Antonio Apolinário Jr.

***Abstract*— This paper investigates the use of the Cubature Kalman Filter (CKF) for estimating the trajectory of a projectile with known ballistic parameters using simulated radar measurements from a Weapon Locating Radar. The CKF is a nonlinear filtering technique with enhanced accuracy and numerical stability compared to the Extended Kalman Filter and the Unscented Kalman Filter. We evaluate the Cubature Kalman Filter performance under realistic measurement noise and dynamic conditions. The simulation results demonstrate improved tracking accuracy and robustness, highlighting its potential as a reliable solution for ballistic trajectory estimation in defense applications.**

***Keywords*— Cubature Kalman Filter, Ballistic Trajectory, Trajectory Estimation, Ballistic Coefficient, Weapon Locating Radar, Impact Point Prediction, Launch Point Prediction.**

I. Introduction

Artillery has long played a decisive role in warfare, from the widespread use of mortars during World War II, where it is estimated that over 50% of infantry casualties were caused by mortar fire [1], to the high-intensity, artillery-centric operations observed in the ongoing Russia-Ukraine conflict [2]. In modern battlefields, artillery is not only a primary source of firepower but also a crucial tool for deterrence, area denial, and rapid response [3].

In this context, the precise computation of ballistic trajectories becomes critical to the effectiveness of defense systems, particularly for technologies like Weapon Locating Radars (WLR). By tracking the launched projectiles in flight, a WLR can accurately locate the hostile weapon and impact point before the projectile reaches the ground, significantly reducing the effectiveness of artillery fire and contributing to the protection of personnel [4]. However, nonlinearities in projectile motion and its observation, wind disturbances, changing atmospheric conditions and measurement noise in radar systems, pose significant challenges to traditional estimation techniques. Addressing these limitations demands advanced and robust algorithms capable of providing accurate and consistent predictions in real-world operational environments.

Kalman filtering techniques are widely employed for state estimation in linear systems [5]. For nonlinear systems, the Extended Kalman Filter (EKF), introduced in [6] and [7], is a commonly used approach that linearizes the system dynamics around the current state estimate. However, this linearization can introduce significant errors, especially in systems with strong nonlinearities [8].

The Unscented Kalman Filter (UKF) addresses some limitations using a deterministic sampling strategy to propagate mean and covariance through nonlinear transformations [9]. Despite this improvement, the UKF's performance is sensitive to selecting sigma point parameters. In contrast, the Cubature Kalman Filter (CKF), which relies on third-degree spherical-radial cubature integration, provides a more accurate and numerically stable alternative for nonlinear state estimation [10].

Several studies have explored advanced filtering techniques to address the nonlinearities involved in ballistic trajectory estimation. For instance, [11] compared the EKF, UKF, and CKF for tracking a ballistic target during the re-entry phase. Similarly, [12] conducted a performance comparison of five types of nonlinear filters in the task of ballistic missile tracking during the re-entry. In contrast, the present work investigates the application of the CKF for estimating the trajectory of artillery projectiles using simulated WLR measurements in shorter detection windows. A comparative study with EKF and UKF evaluates accuracy and robustness under realistic measurement noise conditions.

The remainder of this paper is organized as follows. Section II presents the ballistic trajectory model with associated states and measurement equations. Section III describes the CKF and its application to trajectory estimation. Section IV outlines the simulation setup and discusses the results obtained from the Monte Carlo experiments. Finally, Section V concludes the paper with a summary of the findings and suggestions for future research.

II. Ballistic Trajectory Model

Several models can describe projectile motion, ranging from simple kinematic equations to high-fidelity six-degree-of-freedom (6-DoF) models incorporating detailed aerodynamic, rotational, and structural characteristics [13]. However, in the context of WLR, the point-mass approximation offers a practical and effective solution. This is primarily due to the limited availability of detailed information about the physical and aerodynamic properties of hostile projectiles and the lack of knowledge about their launch platform parameters.

The point-mass approximation ballistic model adopted in this work assumes that the projectile behaves as a rigid body without rotational dynamics and that its motion is governed exclusively by external forces, namely gravitational

Daniel Miñan de Oliveira Crus, Program of Defense Engineering, Military Institute of Engineering (IME), Rio de Janeiro-RJ, e-mail: minan.daniel@ime.eb.br; João Abdalla Ney da Silva, Army Technological Center (CTEx), Rio de Janeiro-RJ, e-mail: jabdallaney@gmail.com. José Antonio Apolinário Jr., Department of Electrical Engineering, Military Institute of Engineering (IME), Rio de Janeiro-RJ, e-mail: apolin@ime.eb.br.

acceleration and aerodynamic drag. An exception applies to rocket trajectories, for which a constant thrust is considered during the burn phase, introducing an internal propulsive force incorporated into the dynamic model. Unlike simplified models with constant gravity, this formulation accounts for gravitational acceleration variations as a function of latitude. Air density and the speed of sound are modeled using an exponential approximation, providing a sufficiently accurate representation of atmospheric effects. Additionally, Earth's curvature and Coriolis effects are neglected, as their influence is minimal for the short- to medium-range trajectories typically associated with RAM (rocket, artillery, and mortar) projectiles.

The point-mass model of a projectile is described by [14]:

$$\frac{d\vec{V}}{dt} = -\frac{\rho S C_d(M)}{2m}\|\vec{V}\|\vec{V} + \vec{g}, \tag{1}$$

where $\vec{V}$ is the projectile's velocity vector, m is the projectile's mass, ρ is the air density, S is the cross-sectional area, $\vec{g}$ is the acceleration vector due to gravity, and $C_d(M)$ denotes the drag coefficient as a function of the Mach number M.

The air density is approximated as an exponential function of altitude [14]:

$$\rho(h) = \rho_0 e^{-\frac{h}{H}}, \tag{2}$$

where $\rho_0 = 1.225$ kg/m^3 is the air density at sea level, h is the projectile's altitude in meters, and $H \approx 8{,}400$ m is the air density decay factor of the atmosphere.

The ballistic coefficient, denoted as $C_B(M)$, characterizes both the fixed physical properties and the aerodynamic efficiency of a projectile. It is defined as a function of the Mach number M, the ratio between the projectile's speed and the local speed of sound, as follows [15]:

$$C_B(M) = \frac{2m}{C_d(M)S} \tag{3}$$

Using $C_B(M)$ instead of separate parameters improves numerical conditioning in filters for ballistic parameter estimation or classification, as its magnitude is comparable to position and velocity states, aiding convergence [16].

Figure 1 illustrates curves of C_d and C_B as functions of M. These curves are commonly determined from wind tunnel experiments, computational fluid dynamics (CFD) simulations, or identified from real flight test data [17] and are typically tabulated for use in ballistic models.

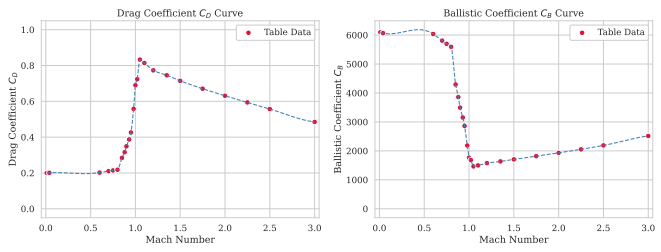

Fig. 1. Example curves of drag coefficient (C_d, dimensionless) and ballistic coefficient (C_B, in kg/m^2) as functions of Mach number (M).

For trajectory estimation, the system state vector includes both position and velocity components:

$$\mathbf{x} = [x,\ y,\ z,\ v_x,\ v_y,\ v_z]^T, \tag{4}$$

where (x, y, z) represents the projectile's position in an inertial reference frame, and (v_x, v_y, v_z) are the corresponding velocity components.

Radar noisy measurements provide the range (r), azimuth (θ), and elevation (ϕ), grouped as:

$$\mathbf{p} = [r,\ \theta,\ \phi]^T, \tag{5}$$

which are converted to Cartesian coordinates using the transformation:

$$\begin{bmatrix} x \\ y \\ z \end{bmatrix} = r \begin{bmatrix} \cos(\phi)\cos(\theta) \\ \cos(\phi)\sin(\theta) \\ \sin(\phi) \end{bmatrix}. \tag{6}$$

III. Cubature Kalman Filter for Trajectory Estimation

Unlike linearization-based approaches such as the EKF, the CKF offers improved estimation accuracy in strongly nonlinear systems. In various applications, it also has demonstrated superior performance and numerical stability compared to the UKF in a wide range of applications [18].

We assume a dynamic system with the following form:

$$\text{Process equation:} \quad \mathbf{x}_k = \mathbf{f}(\mathbf{x}_{k-1}, \mathbf{u}_{k-1}) + \mathbf{v}_{k-1} \tag{7}$$

$$\text{Measurement equation:} \quad \mathbf{z}_k = \mathbf{h}(\mathbf{x}_k, \mathbf{u}_k) + \mathbf{w}_k \tag{8}$$

where $\mathbf{f}(\cdot)$ and $\mathbf{h}(\cdot)$ are nonlinear functions, and $\mathbf{v}_{k-1}$ and $\mathbf{w}_k$ denote the process and measurement noises, respectively.

The CKF algorithm, given the known initial values $\mathbf{x}_0$, $\mathbf{P}_{0|0}$, and the ballistic coefficient curve $C_B(M)$, involves the following steps [19]:

Time Update

- Assuming at time k that the posterior density function

$$p(\mathbf{x}_{k-1}|D_{k-1}) = \mathcal{N}(\hat{\mathbf{x}}_{k-1|k-1}, \mathbf{P}_{k-1|k-1})$$

is known and n_x is the number of states. Factorize:

$$\mathbf{P}_{k-1|k-1} = \mathbf{S}_{k-1|k-1}\mathbf{S}_{k-1|k-1}^\top \tag{9}$$

- Evaluation of cubature points $(i = 1, 2, \ldots, c)$:

$$\mathbf{X}_{i,k-1|k-1} = \mathbf{S}_{k-1|k-1}\boldsymbol{\xi}_i + \hat{\mathbf{x}}_{k-1|k-1} \tag{10}$$

where $c = 2n_x$, $\mathbf{e}_i$ stands for the i-th coordinate vector in $\mathbb{R}^n$ and the cubature points are defined by [18]:

$$\boldsymbol{\xi}_i := \begin{cases} \sqrt{\frac{c}{2}}\,\mathbf{e}_i, & i = 1, 2, \ldots, n_x, \\ -\sqrt{\frac{c}{2}}\,\mathbf{e}_{i-n_x}, & i = n_x+1, n_x+2, \ldots, c, \end{cases} \tag{11}$$

- Evaluation of propagated cubature points

$$\mathbf{X}^*_{i,k|k-1} = \mathbf{f}(\mathbf{X}_{i,k-1|k-1}, \mathbf{u}_{k-1}) \tag{12}$$

- Estimation of predicted state:

$$\hat{\mathbf{x}}_{k|k-1} = \frac{1}{c}\sum_{i=1}^{c} \mathbf{X}^*_{i,k|k-1} \tag{13}$$

- Estimation of predicted error covariance:

$$\mathbf{P}_{k|k-1} = \frac{1}{c}\sum_{i=1}^{c} \mathbf{X}^*_{i,k|k-1}\mathbf{X}^{*T}_{i,k|k-1} - \hat{\mathbf{x}}_{k|k-1}\hat{\mathbf{x}}^\top_{k|k-1} + \mathbf{Q}_{k-1} \tag{14}$$

Measurement Update

- Factorize

$$\mathbf{P}_{k|k-1} = \mathbf{S}_{k|k-1}\mathbf{S}_{k|k-1}^{\top} \tag{15}$$

- Evaluation of cubature points $(i = 1, 2, \ldots, c)$

$$\mathbf{X}_{i,k|k-1} = \mathbf{S}_{k|k-1}\boldsymbol{\xi}_i + \hat{\mathbf{x}}_{k|k-1} \tag{16}$$

- Evaluation of propagated cubature points $(i = 1, 2, \ldots, c)$

$$\mathbf{Z}_{i,k|k-1} = \mathbf{h}(\mathbf{X}_{i,k|k-1}, \mathbf{u}_k) \tag{17}$$

- Estimation of predicted measurement

$$\hat{\mathbf{z}}_{k|k-1} = \frac{1}{c}\sum_{i=1}^{c}\mathbf{Z}_{i,k|k-1} \tag{18}$$

- Estimation of innovation covariance matrix

$$\mathbf{P}_{zz,k|k-1} = \frac{1}{c}\sum_{i=1}^{c}\mathbf{Z}_{i,k|k-1}\mathbf{Z}_{i,k|k-1}^{\top} - \hat{\mathbf{z}}_{k|k-1}\hat{\mathbf{z}}_{k|k-1}^{\top} + \mathbf{R}_k \tag{19}$$

- Estimation of cross-covariance matrix

$$\mathbf{P}_{xz,k|k-1} = \frac{1}{c}\sum_{i=1}^{c}\mathbf{X}_{i,k|k-1}\mathbf{Z}_{i,k|k-1}^{\top} - \hat{\mathbf{x}}_{k|k-1}\hat{\mathbf{z}}_{k|k-1}^{\top} \tag{20}$$

- Estimation of Kalman gain

$$\mathbf{W}_k = \mathbf{P}_{xz,k|k-1}\mathbf{P}_{zz,k|k-1}^{-1} \tag{21}$$

- Estimation of updated state

$$\hat{\mathbf{x}}_{k|k} = \hat{\mathbf{x}}_{k|k-1} + \mathbf{W}_k(\mathbf{z}_k - \hat{\mathbf{z}}_{k|k-1}) \tag{22}$$

- Estimation of corresponding error covariance

$$\mathbf{P}_{k|k} = \mathbf{P}_{k|k-1} - \mathbf{W}_k\mathbf{P}_{zz,k|k-1}\mathbf{W}_k^{\top} \tag{23}$$

The CKF algorithm [19] above was implemented in Python, alongside conventional EKF and UKF approaches, to assess their performance in meeting the requirements of a WLR.

IV. Simulation and Results

To evaluate the performance of the proposed estimation algorithms, we developed a ballistic trajectory simulator using the point-mass model. The simulator incorporates gravitational effects with latitude-dependent variation and models atmospheric conditions using exponential approximations for air density and speed of sound.

Digital elevation terrain maps might be incorporated to enable more accurate modeling of projectile-to-ground interaction and improving the estimation of both the launch point (LP) and impact point (IP) [20]. In this work, the terrain was modeled as a planar surface with zero elevation, and both the LP and IP were assumed to lie on it.

Radar measurements for each projectile were processed using EKF, UKF, and CKF algorithms. The evaluation focused on key performance metrics, including the accuracy of LP and IP predictions and computational efficiency, particularly within the limited time available for early warning and counterfire after WLR detection.

Three distinct classes of RAM projectiles were selected to evaluate the estimation performance of the algorithms. Each projectile was characterized by different physical and aerodynamic parameters, including mass, cross-sectional area, and ballistic coefficient. Table I summarizes the main characteristics of each projectile used in the simulation.

TABLE I
PROJECTILE PARAMETERS

Parameter	**P1**	**P2**	**P3**
Class	Medium Mortar	Heavy Howitzer	Light Rocket
Caliber	81 mm	155 mm	70 mm
Cross-sect. Area (m^2)	0.00515682	0.01879622	0.00384845
Mass (kg)	4.2	43.4	11.9
Muzzle Velocity (m/s)	301.9	684.3	97.9
Max Velocity (m/s)	301.9	684.3	811.6
Firing Angle (deg)	60	45	33
Time of Flight (s)	30.11	69.64	40.11
Burn Time (s)	-	-	1.17

The radar system was modeled with parameters representative of modern WLRs. Table II presents the main simulation settings for radar measurement generation.

TABLE II
RADAR SIMULATION PARAMETERS

Parameter	**Value**
Update Rate	10 Hz
Range Accuracy (1σ)	10 m
Azimuth Accuracy (1σ)	2 mrad
Elevation Accuracy (1σ)	2 mrad
Radar-weapon distance	14 km

To evaluate the performance of the CKF, a Monte Carlo simulation with 100 independent runs was conducted and compared against EKF and UKF in the prediction of both LP and IP. The simulation setup assumes a projectile with a known ballistic coefficient tracked by a WLR. It employs the same dynamic model, initial conditions, and forward/backward extrapolation strategy described in [20] for processing the set of radar measurements.

To quantitatively evaluate the accuracy of the estimated LP and IP, the Circular Error Probable (CEP) metric was adopted. $\text{CEP}_{50\%}$ is a widely used measure in ballistics and target tracking, defined as the radius of a circle centered at the true point within which 50% of the estimated positions fall [21]. This metric intuitively and statistically represents localization accuracy in 2D space, making it well-suited for military and radar applications, where estimation errors are typically circular and Gaussian. CEP provides a single scalar value that facilitates performance comparison across scenarios and filters.

Figure 2 illustrates the 3D trajectory predictions for projectiles P1, P2, and P3, comparing the estimated paths obtained by forward and backward propagation against the true trajectory. The radar measurements are shown as discrete blue points, and the estimated LP and IP are indicated. Each case uses a measurement window at a different flight phase relative to the apogee.

Figures 3, 4, and 5 present the simulation results regarding $\text{CEP}_{50\%}$ for projectiles P1, P2, and P3, respectively. The CKF achieved the lowest $\text{CEP}_{50\%}$ values in all cases, remaining below 2% of the distance between the WLR and the corresponding true LP or IP. These results reflect a high

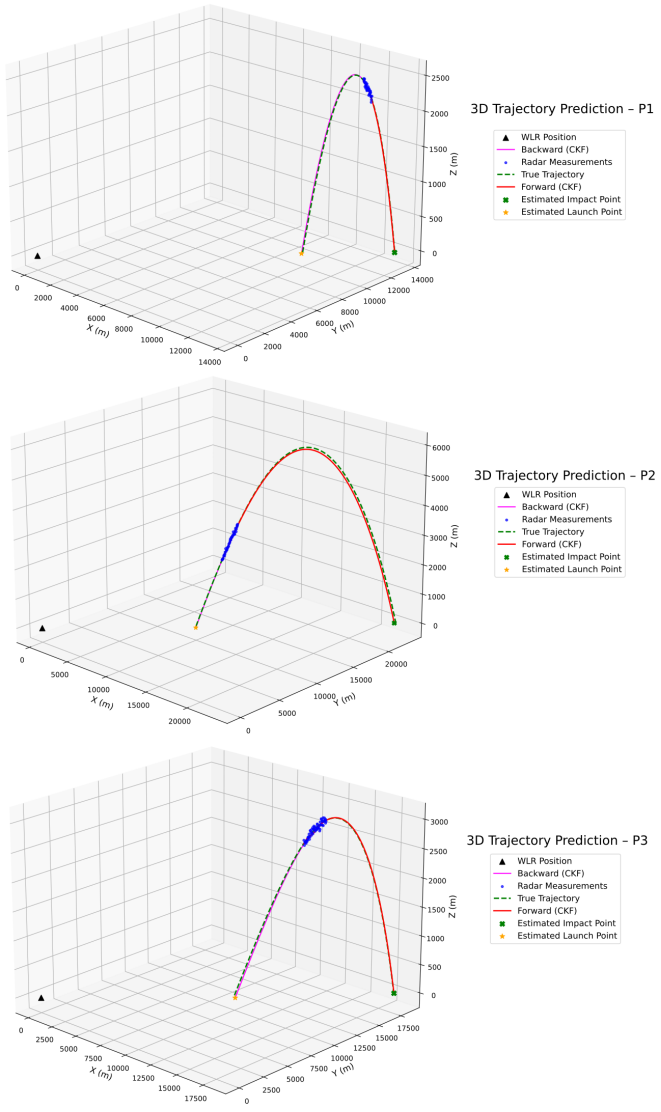

Fig. 2. Predicted and true trajectories in 3D space for projectiles P1, P2, P3 and radar measurements.

level of positional accuracy, with the UKF also demonstrating relatively competitive performance. Overall, the CKF and UKF outperformed the EKF in all evaluated scenarios due to their greater ability to handle the nonlinearities of the dynamic model without relying on linear approximations, such as the first-order derivatives used in the EKF.

Table III summarizes the $CEP_{50\%}$ values for LP and IP estimations across all projectiles and filtering methods.

TABLE III
$CEP_{50\%}$ VALUES FOR LAUNCH AND IMPACT POINT ESTIMATIONS

Prediction	Filter	P1	P2	P3
LP	EKF	571.59 m	214.07 m	697.11 m
	UKF	378.12 m	139.98 m	401.66 m
	CKF	**141.76 m**	**62.10 m**	**112.19 m**
IP	EKF	227.37 m	562.41 m	448.27 m
	UKF	142.67 m	380.17 m	280.29 m
	CKF	**62.97 m**	**168.12 m**	**65.65 m**

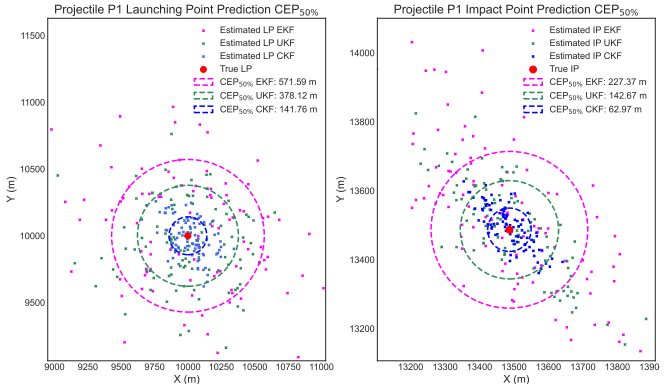

Fig. 3. Comparison of $CEP_{50\%}$ values for projectile P1.

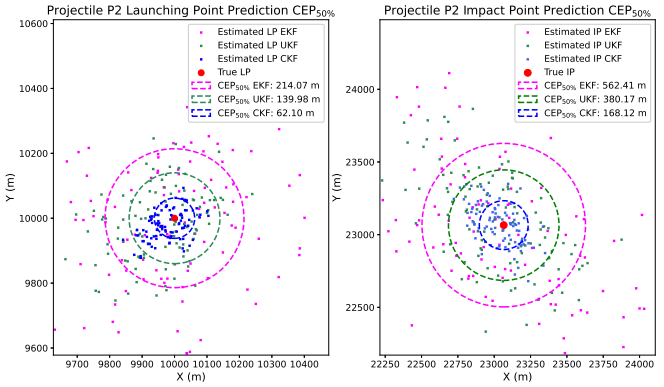

Fig. 4. Comparison of $CEP_{50\%}$ values for projectile P2.

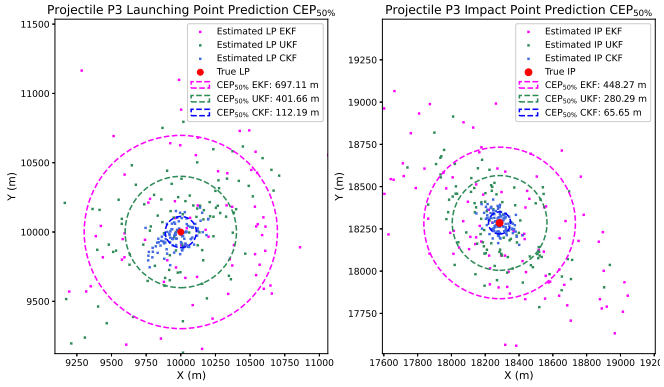

Fig. 5. Comparison of $CEP_{50\%}$ values for projectile P3.

Table IV summarizes the average execution time for each filtering algorithm. As expected, the EKF presented the lowest computational cost due to its linearization approach and reduced mathematical complexity. In contrast, the CKF and UKF require multiple function evaluations for each update step, resulting in longer processing times. However, both remained suitable for real-time applications.

The relative position of the radar detection window with respect to the projectile's apogee significantly influences the estimation accuracy. When measurements are taken near the apogee, as in the cases of P1 and P3, both forward and back-

TABLE IV
AVERAGE EXECUTION TIME FOR LP AND IP PREDICTION

Technique	Execution Time (ms)
EKF	73 ms
UKF	231 ms
CKF	244 ms

ward extrapolations benefit from symmetrical observability, leading to balanced accuracy in estimating both launch and impact points. In contrast, P2 is observed before the apogee, improving LP estimation due to proximity but limiting the information available to reconstruct the later portion of the trajectory. This asymmetry increases IP errors, as reflected in the $\text{CEP}_{50\%}$ results. These findings highlight the importance of radar observation timing in WLR performance and estimation reliability.

V. CONCLUSION

This study investigated the application of the CKF for estimating ballistic projectile trajectories using simulated radar measurements from a WLR. The performance of the CKF was compared with that of the EKF and the UKF across three scenarios, focusing on the accuracy of LP and IP predictions.

The CKF provided the best overall performance, maintaining estimation errors below 2% of the projectile-to-radar distance while offering acceptable computational efficiency for real-time applications. Results indicate a substantial improvement in estimation accuracy compared to both UKF and EKF. Across all scenarios, the CKF reduced the $\text{CEP}_{50\%}$ by approximately 2 to 4 times relative to the UKF and about 3 to 6 times compared to the EKF.

These findings highlight the advantages of the CKF in achieving higher accuracy and robustness, particularly in the presence of significant measurement noise and nonlinear dynamics. Despite the increased computational load compared to the EKF, the CKF demonstrated a favorable balance between estimation accuracy and processing time [18], confirming its viability for real-time implementation.

A key limitation of the proposed approach lies in the assumption of a known ballistic coefficient for the projectile. This constraint, however, can be mitigated through projectile classification techniques based on initial radar measurements [22], enabling the selection of an appropriate ballistic coefficient from a predefined database. Alternatively, the ballistic coefficient curve can be extracted from prior detection data using filtering techniques, which allow for a more accurate estimation even under measurement uncertainty. These strategies are currently under investigation as part of ongoing efforts to extend the capabilities of the estimation framework.

Future work will involve conducting real-world experiments with live radar data to validate and possibly refine the proposed methodologies, investigating advanced filtering techniques to enhance estimation accuracy like fifth-degree CKF (5TH-CKF) [23], and implementing computational optimizations to ensure effective real-time performance.

ACKNOWLEDGEMENTS

The authors would like to thank the Brazilian Navy and Brazilian Army for partial support of this work, which was also partially funded by the FINEP Project 0 1 22 0329 00.

REFERENCES

[1] J. Milner, "Radar mortar locator development in the UK: the first 30 years," in *IEE Proceedings F (Communications, Radar and Signal Processing)*, vol. 131, no. 2. IET, 1984, pp. 233–239.
[2] L.-G. Oprean, "Artillery and drone action issues in the war in Ukraine," *Scientific Bulletin*, vol. 28, no. 1, p. 55, 2023.
[3] J. Bailey, "Artillery and warfare 1945-2025," 2009.
[4] W. Fishbein, "Firefinder, a radar forty years in the making," *IEEE Transactions on Aerospace and Electronic Systems*, vol. 44, no. 2, pp. 817–829, 2008.
[5] R. E. Kalman, "A new approach to linear filtering and prediction problems," *Journal of Basic Engineering*, vol. 82, no. 1, pp. 35–45, Mar. 1960.
[6] R. E. Larson, R. M. Dressler, and R. S. Ratner, *Application of the extended Kalman filter to ballistic trajectory estimation*. Stanford Research Institute, 1967.
[7] M. Gruber, *An approach to target tracking*. MIT Lincoln Laboratory, 1967.
[8] F. Daum, "Nonlinear filters: beyond the Kalman filter," *IEEE Aerospace and Electronic Systems Magazine*, vol. 20, no. 8, pp. 57–69, 2005.
[9] S. J. Julier and J. K. Uhlmann, "Unscented filtering and nonlinear estimation," *Proceedings of the IEEE*, vol. 92, no. 3, pp. 401–422, 2004.
[10] I. Arasaratnam and S. Haykin, "Cubature Kalman filters," *IEEE Transactions on Automatic Control*, vol. 54, no. 6, pp. 1254–1269, 2009.
[11] D. Hong-de, D. Shao-wu, C. Yuan-cai, and W. Guang-bin, "Performance comparison of EKF/UKF/CKF for the tracking of ballistic target," *TELKOMNIKA Indonesian Journal of Electrical Engineering*, vol. 10, no. 7, 2012.
[12] N. K. Singh, S. Bhaumik, and S. Bhattacharya, "A comparison of several nonlinear filters for ballistic missile tracking on re-entry," in *2016 IEEE First International Conference on Control, Measurement and Instrumentation (CMI)*. IEEE, 2016, pp. 459–463.
[13] G. Klimi, *Exterior Ballistics*. Xlibris Corporation, 2014.
[14] R. McCoy, *Modern exterior ballistics: The launch and flight dynamics of symmetric projectiles*. Schiffer Pub., 1999.
[15] F. J. Regan, *Dynamics of atmospheric re-entry*. Aiaa, 1993.
[16] S. D. M. Achanta, "Analysis of effect of ballistic coefficient in the formulations and performance of EKF with emphasis on air drag," *Indian Journal of Science and Technology*, vol. 8, pp. 1–5, 01 2015.
[17] Y. Chen, C. Wen, Z. Gong, and M. Sun, "Drag coefficient curve identification of projectiles from flight tests via optimal dynamic fitting," *Control Engineering Practice*, vol. 5, no. 5, pp. 627–636, May 1997.
[18] I. Arasaratnam, "Cubature Kalman Filtering Theory & Applications," Thesis, McMaster University, Apr. 2009.
[19] I. Arasaratnam and S. Haykin, "Cubature Kalman Filters," *IEEE Transactions on Automatic Control*, vol. 54, no. 6, pp. 1254–1269, Jun. 2009.
[20] D. M. O. Crus, F. A. C. Bastos, J. A. Apolinário Jr., and J. A. N. Silva, "Performance of backward Kalman filtering techniques for estimating projectile launch point," in *2025 IEEE 16th Latin America Symposium on Circuits and Systems (LASCAS)*, 2025, pp. 1–5.
[21] R. S. Johnson, S. D. Cottrill, and P. Z. Peebles, "A computation of radar SEP and CEP," *IEEE Transactions on Aerospace and Electronic Systems*, vol. AES-5, no. 2, pp. 353–354, 1969.
[22] F. Tennebø, "Improving classification of ballistic, non-cooperative radar targets," Master's thesis, Østfold University College, Norway, 2022.
[23] B. Jia, M. Xin, and Y. Cheng, "High-degree cubature kalman filter," *Automatica*, vol. 49, no. 2, pp. 510–518, 2013.